Accepted Manuscript

A computational method to assess in vivo stresses and unloaded configuration of patient-specific blood vessels

J. Bols, J. Degroote, B. Trachet, B. Verhegghe, P. Segers, J. Vierendeels

PII: S0377-0427(12)00481-5
DOI: 10.1016/j.cam.2012.10.034
Reference: CAM 8951

To appear in: *Journal of Computational and Applied Mathematics*

Received date: 30 January 2012
Revised date: 4 July 2012

Please cite this article as: J. Bols, J. Degroote, B. Trachet, B. Verhegghe, P. Segers, J. Vierendeels, A computational method to assess in vivo stresses and unloaded configuration of patient-specific blood vessels, *Journal of Computational and Applied Mathematics* (2012), doi:10.1016/j.cam.2012.10.034

A computational method to assess in vivo stresses and unloaded configuration of patient-specific blood vessels

J. Bols[a,b,*], J. Degroote[a], B. Trachet[b], B. Verhegghe[b], P. Segers[b], J. Vierendeels[a]

[a]*Department of Flow, Heat and Combustion Mechanics, Ghent University*
Sint-Pietersnieuwstraat 41, B-9000 Ghent, Belgium
[b]*IBiTech-bioMMeda, Ghent University*
De Pintelaan 185, B-9000 Ghent, Belgium

Abstract

In the modelling process of cardiovascular diseases, one often comes across the numerical simulation of the blood vessel wall. When the vessel geometry is patient-specific and obtained in vivo via medical imaging, the stress distribution throughout the vessel wall is unknown. However, simulating the full physiological pressure load inside the blood vessel without incorporating in vivo stresses will result in an inaccurate stress distribution and an incorrect deformation of the vessel wall. In this work a computational method is formulated to restore the zero-pressure geometry of patient-specific blood vessels, and to recover the in vivo stress field of the loaded structures at the moment of imaging. The proposed backward displacement method is able to solve the inverse problem iteratively using fixed point iterations. As only an update of the mesh is required, the formulation of this method allows for a straightforward implementation in combination with existing structural solvers, even if the structural solver is a black box.

Keywords: backward displacement method, inverse modelling, patient-specific blood vessels, in vivo stress, prestress, zero-pressure geometry, image-based modelling

*Corresponding author. T: +32 9 264 33 12
Email addresses: Joris.Bols@UGent.be (J. Bols), Joris.Degroote@UGent.be (J. Degroote), Bram.Trachet@UGent.be (B. Trachet), Benedict.Verhegghe@UGent.be (B. Verhegghe), Patrick.Segers@UGent.be (P. Segers), Jan.Vierendeels@UGent.be (J. Vierendeels)

1. Introduction

Numerical analyses of the cardiovascular system are able to provide medical researchers with information that cannot (easily) be measured in a clinical setting and may contribute to a better comprehension and insight into the pathophysiology of cardiovascular diseases. In addition, numerical models offer a computational environment in which both new and existing medical procedures and devices can be tested and optimized, which is both cost-effective and patient-friendly. The continuous improvement of computational methods, computational power and medical imaging techniques encourages the general belief that computational models will eventually be used in clinical practice, with a trend toward more realistic, patient-specific models. These models cannot do without non-invasive medical imaging techniques such as X-ray computed tomography (CT), magnetic resonance imaging (MRI) and ultrasound imaging which not only allow for accurate in vivo visualization of 3D patient-specific geometries, but also provide information about wall thickness and wall motion. The in vivo data can be used to generate and validate the computational structural dynamics (CSD) model and to fit material parameters of a constitutive law to mimic the patient-specific behavior of the aortic wall [1]. When the interaction between the blood flow and the arterial wall is taken into account, MRI and ultrasound provide valuable information for patient-specific boundary conditions of the fluid domain in a fluid-structure interaction (FSI) simulation.

It is important to realize that, at the moment of medical image acquisition, a physiological pressure load is present in the arterial system. When using the in vivo obtained patient-specific geometry to model the arterial wall, this arterial structure therefore does not correspond to the unloaded configuration and there is an in vivo stress and strain field present in the vessel wall. Neglecting their presence results in incorrect values for the stress and the deformation when simulating the internal pressure load inside cardiovascular structures in general and inside cerebral and aortic aneurysms in particular [2, 3, 4, 5, 6].

It is not possible to measure (in vivo) the unloaded configuration of the blood vessel or the stress distribution throughout the arterial wall. However, when the in vivo measured geometry and the corresponding blood pressure at the moment of imaging are known, an inverse problem can be defined to solve for the zero-pressure geometry or the in vivo stress field. Note that this inverse problem and its solution methods to reveal the load free configuration are not limited to the field of biomechanics. For example in mechanical production and design applications, the desired shape of manufacturing tools, gaskets, rubber seals and even turbine

blades has to be reached under loading conditions [7, 8, 9].

In this paper a fixed point method is presented to solve for the zero-pressure geometry by iteratively updating the nodal coordinates of the geometry towards the unknown unloaded configuration. As only an update of the nodal coordinates is required, the method in section 2 allows for a straightforward implementation in combination with existing finite element solvers, even if the solver is a black box and there is no access to the source code. In section 3 the zero-pressure geometry is calculated for two different models. Applying the measured arterial pressure in a forward analysis fully recovers their in vivo measured geometry and restores their in vivo present stress state.

2. Methods

2.1. Problem description

Before defining the inverse problem, a general forward problem is formulated. Therefore, we define a stress free reference configuration by

$$\Omega(\boldsymbol{X}, \mathbf{0}) \tag{1}$$

in which $\boldsymbol{X}$ denotes the material coordinates of the undeformed reference geometry, and where the second argument of the configuration Ω refers to the zero stress state that corresponds to this unloaded reference configuration. Then, a forward analysis can be defined as the calculation of the equilibrium configuration

$$\Omega(\boldsymbol{x}, \boldsymbol{\sigma}) \tag{2}$$

with $\boldsymbol{x}$ the coordinates of the deformed geometry and $\boldsymbol{\sigma}$ the second-order stress tensor. As shown in Figure 1, this deformed configuration results from a pressure load p, applied at the inner surface of the undeformed blood vessel wall,

$$p = -\boldsymbol{\tau}.\boldsymbol{n} = -(\boldsymbol{\sigma}.\boldsymbol{n}).\boldsymbol{n}$$

with $\boldsymbol{n}$ the outward unit normal vector, and a zero traction vector ($\boldsymbol{\tau} = \mathbf{0}$) at the outer surface of this undeformed reference state (1). Furthermore, the nodes at the ending cross sections are only allowed to move in radial direction with respect to the local centerline

$$\begin{cases} U_\theta = 0 \\ U_z = 0 \end{cases} \tag{3}$$

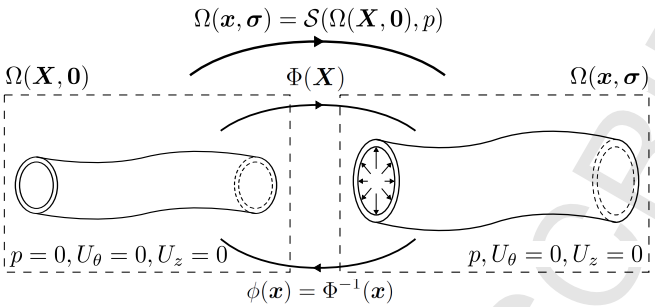

Figure 1: Schematic representation and notations.

To be in equilibrium, the equilibrium conditions, the compatibility requirements and the presence of an appropriate material model, which sets the relation between the stress field and the strain field, are satisfied. The equilibrium configuration (2) can be computed by a structural solver, which we denote by $\mathcal{S}$. Using these definitions, we define the forward analysis by

$$\Omega(\boldsymbol{x},\boldsymbol{\sigma}) = \mathcal{S}(\Omega(\boldsymbol{X},\boldsymbol{0}),p) \tag{4}$$

The deformation can be defined by the forward mapping $\Phi : \boldsymbol{X} \mapsto \boldsymbol{x}$ and the deformation gradient tensor $\boldsymbol{F}$

$$\boldsymbol{x} = \Phi(\boldsymbol{X}) \tag{5a}$$

$$\boldsymbol{F} = \frac{\partial \boldsymbol{x}}{\partial \boldsymbol{X}} = \frac{\partial \Phi(\boldsymbol{X})}{\partial \boldsymbol{X}} \tag{5b}$$

The inverse or backward problem calculates the undeformed reference geometry that corresponds to a given geometry, which is deformed due to a pressure load. Therefore, in Figure 1, we now assume

$$\begin{cases} \boldsymbol{X} = \boldsymbol{X}^* \\ \boldsymbol{\sigma} = \boldsymbol{\sigma}^* \end{cases}, \qquad \begin{cases} \boldsymbol{x} = \boldsymbol{x}_m \\ p = p_m \end{cases}$$

where $\boldsymbol{X}^*$ and $\boldsymbol{\sigma}^*$ are the zero-pressure geometry present in the undeformed reference configuration and the stress state present in the in vivo configuration, i.e. the unknown variables of this inverse problem. The in vivo geometry $\boldsymbol{x}_m$ and the internal pressure load p_m are the known input parameters for the inverse problem, where the subscript m refers to (in vivo) measurements.

Then, the backward problem can be formulated as follows:
Find the in vivo configuration

$$\Omega(\boldsymbol{x}_m, \boldsymbol{\sigma}^*) \tag{6}$$

which is yet unknown as only $\boldsymbol{x}_m$ is known and $\boldsymbol{\sigma}^*$ is not, and which is in equilibrium with the measured internal pressure load p_m, the zero traction at the outside and the kinematic Dirichlet boundary conditions (3). Therefore, find the corresponding undeformed reference configuration

$$\Omega(\boldsymbol{X}^*, \boldsymbol{0}) \tag{7}$$

so that the in vivo equilibrium configuration (6) can be found by imposing the in vivo measured pressure p_m onto the zero-pressure reference configuration (7) in a forward analysis (4)

$$\Omega(\boldsymbol{x}_m, \boldsymbol{\sigma}^*) = \mathcal{S}(\Omega(\boldsymbol{X}^*, \boldsymbol{0}), p_m) \tag{8}$$

Equation (8) results in the stress tensor field $\boldsymbol{\sigma}^*$ which is defined as the *prestress* introduced by the forward analysis or the *in vivo stress* accompanying the in vivo image-based geometry. The unloaded reference geometry can be written as

$$\boldsymbol{X}^* = \phi(\boldsymbol{x}_m) = \Phi^{-1}(\boldsymbol{x}_m)$$

in which $\phi : \boldsymbol{x} \mapsto \boldsymbol{X}$ denotes the inverse deformation mapping. This allows to obtain the original in vivo geometry at the moment of imaging $\boldsymbol{x}_m$ using the in (5a) proposed forward deformation of the zero-pressure geometry $\boldsymbol{X}^*$

$$\Phi(\boldsymbol{X}^*) = \Phi(\phi(\boldsymbol{x}_m)) = \Phi(\Phi^{-1}(\boldsymbol{x}_m)) = \boldsymbol{x}_m$$

2.2. Backward displacement method

This paper proposes a method to solve for the zero-pressure geometry and the in vivo stress state by means of fixed point iterations. The algorithm makes use of a forward analysis to update the approximate zero-pressure geometry, while evaluating the residual as the maximum distance that is still present between the image-based geometry and the geometry resulting from this forward problem. When convergence is reached (i) a zero-pressure geometry is found and (ii) the resulting in vivo measured geometry is recovered and in equilibrium with an in vivo stress field and the in vivo load. Furthermore, only the nodal coordinates of the mesh need to be updated before every iteration, allowing for a straightforward implementation in combination with existing structural solvers, even if the solver

Algorithm 1 FIXED POINT ALGORITHM TO RECOVER THE ZERO-PRESSURE GEOMETRY AND THE IN VIVO STRESS TENSOR FIELD

1: $i = 0$
2: $\boldsymbol{X}^1 = \boldsymbol{x}_m$
3: **while** $i = 0$ or $r^i_{max} \geq \epsilon$ **do**
4: $\quad i = i + 1$
5: $\quad \Omega(\boldsymbol{x}^i, \boldsymbol{\sigma}^i) = \mathcal{S}(\Omega(\boldsymbol{X}^i, \boldsymbol{0}), p_m)$
6: $\quad \boldsymbol{U}^i = \boldsymbol{x}^i - \boldsymbol{X}^i$
7: $\quad \boldsymbol{X}^{i+1} = \boldsymbol{x}_m - \boldsymbol{U}^i$
8: **end while**
9: Zero-pressure reference geometry $\boldsymbol{X}^* = \boldsymbol{X}^i$
10: In vivo stress tensor $\sigma^* = \boldsymbol{\sigma}^i$

is a black box and no access is granted to the source code (as is the case with most commercial packages).

The fixed point algorithm to recover this zero-pressure geometry and the in vivo stress tensor field is shown in Algorithm 1. It starts by initializing an approximation for the zero-pressure geometry $\boldsymbol{X}^{i=1}$. As initial guess, the original image-based geometry $\boldsymbol{x}_m$ is chosen. Then, a fixed point based iterative procedure is performed until convergence is reached. First, the structural solver calculates an equilibrium configuration $\Omega(\boldsymbol{x}^i, \boldsymbol{\sigma}^i)$ from the intermediate reference configuration $\Omega(\boldsymbol{X}^i, \boldsymbol{0})$ loaded with the full in vivo pressure load p_m. The displacements of the material points in the forward analysis are denoted by $\boldsymbol{U}^i$. Finally, the approximation of the zero-pressure geometry ($\boldsymbol{X}^i$) is updated by subtracting the nodal displacements $\boldsymbol{U}^i$ from the *original* image-based coordinates $\boldsymbol{x}_m$. This procedure leads to an update of the mesh $\boldsymbol{X}^{i+1}$ (step 7 in Algorithm 1) which is used in the next iteration or, if convergence is reached, to the zero-pressure geometry $\boldsymbol{X}^*$. Furthermore, the forward analysis calculates the stress state $\boldsymbol{\sigma}^i$ (step 5 in Algorithm 1) which is left unused throughout the algorithm but represents the in vivo stress tensor $\boldsymbol{\sigma}^*$ present in the in vivo measured geometry upon convergence. A residual

$$r^i_j = \|\boldsymbol{x}_{m,j} - \boldsymbol{x}^i_j\|_2 \qquad , \quad \forall j \in [1, N] \tag{9}$$

is defined as the distance between the coordinates of the j^{th} node in the i^{th} deformed geometry $\boldsymbol{x}^i_j$ and in the original image based geometry $\boldsymbol{x}_{m,j}$. Where $\|.\|_2$ stand for the L^2-norm and N represents the total number of nodes in the model.

Convergence is reached when the maximum residual

$$r^i_{max} = \max_{j\in[1,N]}\{r^i_j\} \tag{10}$$

is lower than the convergence criterion ϵ.

2.3. Existing solution methods

Besides the method proposed in this paper, there exist other techniques to incorporate in vivo stress into computational models of the cardiovascular system, given the in vivo image-based geometry $\boldsymbol{x}_m$ and internal pressure load p_m.

Raghavan et al. were the first to take into account a non-invasively determined zero-pressure geometry in the numerical modelling process of an abdominal aortic aneurysm (AAA) [10]. Therefore, they developed an optimization framework for the parameter k such that the coordinates of the unknown zero-pressure reference geometry $\boldsymbol{X}^*$ can be approximated by $(\boldsymbol{x}_m - k\boldsymbol{U})$, where $\boldsymbol{U}$ represents the nodal displacements that result from a single forward calculation in which the lumen pressure load is applied onto the in vivo measured reference geometry $\boldsymbol{x}_m$.

Lu et al. introduced the inverse elastostatic method, originally described by Govindjee and Mihalic [7, 8], to the field of cardiovascular biomechanics as another way to calculate the zero-pressure geometry [2]. The implementation, however, requires access to the finite element code what can be seen as a drawback.

Gee et al. implemented previous strategy as the Inverse Design (ID) method, and compared this prestressing technique with another method, the so called Modified Updated Lagrangian Formulation (MULF) [4, 11]. The methodology used, is similar to the Backward Incremental (BI) method introduced by de Putter et al. [3]. In contrast to the backward displacement method, described in this paper, the zero-pressure geometry is not calculated directly but the equilibrium configuration $\Omega(\boldsymbol{x}_m, \boldsymbol{\sigma}^*)$ is computed instead. By incrementally increasing the pressure load towards the full in vivo pressure p_m while discarding the corresponding deformations ($\boldsymbol{x}^i = \boldsymbol{x}_m$) a prestressed ($\boldsymbol{\sigma}^*$) and prestrained configuration is generated. The procedure calculates the new stress tensor field $\boldsymbol{\sigma}^i$ that will be used at the next increment by loading the i^{th} non-equilibrium configuration $\Omega(\boldsymbol{x}_m, \boldsymbol{\sigma}^{i-1})$ with the incrementally increased internal pressure ($p^i = p^{i-1} + \delta p^i$). As such, the stress tensor gets updated towards the in vivo stress tensor and the strain tensor gets implicitly updated by a multiplicative split of the deformation gradient tensor $\boldsymbol{F}_{0,i} = \boldsymbol{F}_{0,i-1}.\boldsymbol{F}_{i-1,i}$ [5, 12]. Afterwards, the zero-pressure geometry can be constructed by reducing the luminal pressure to 0 Pa [13]. According to [3] the

last pressure increment has to be chosen extremely small to return a final equilibrium configuration. The method allows the use of a black box structural solver if the finite element code is able to update the initial stress tensor field with each iteration. A similar approach of prestressing was used earlier by Pinsky et al. to include the internal stress state in the cornea under the presence of the full intraocular pressure load through a fixed point iteration instead of increasing the pressure incrementally [14].

As the effect of viscous forces would be small, the zero-pressure geometry or the in vivo stress state resulting from one of the above methods, which only involve a structural model of the cardiovascular region of interest, can also be used in FSI models. Bazilevs et al., however, report that the viscous effect is not negligible and account for the viscous traction caused by the blood flow when solving the balance of linear momentum for the solid [15]. Therefore, a separate steady flow CFD simulation with rigid walls is performed to obtain the fluid traction vector. After the iterative calculation of the prestress component $\boldsymbol{S}_0$ of the additive decomposition $(\boldsymbol{S} + \boldsymbol{S}_0)$ of the second Piola-Kirchhoff stress tensor it is used as initial stress in their in vivo geometry based FSI model [16].

3. Examples

This section focuses on two examples. In the first example a simplified model of a small artery is used for validation purpose and to evaluate the importance of the correct stress incorporation in the in vivo measured geometry. The second example concerns a mouse-specific abdominal aorta with four side branches to explore the ability of the backward displacement method to restore a more complex cardiovascular structure at its zero-pressure state. In both examples the calculations were performed using the commercial finite element analysis software Abaqus/Standard (Simulia). However, as stated earlier, any other structural mechanics solver can be used using any discretisation method, element types and shape functions.

3.1. Example 1: in vivo stress incorporation in a thick-walled cylinder

A small unloaded artery is modelled using a straight cylindrical tube with a length of 10 mm, an inner radius of 0.5 mm and a wall thickness to diameter ratio of 0.15. The boundary conditions only allow a radial displacement at the ending cross sections. The geometrical model is discretized using $64 \times 32 \times 4$ quadratic hexahedral elements with reduced integration and a hybrid formulation.

The vessel wall behaviour is modelled by an incompressible isotropic hyperelastic material using the polynomial strain energy density function

$$W = C_{10}(I_1 - 3) + C_{01}(I_2 - 3) + C_{20}(I_1 - 3)^2 + C_{11}(I_1 - 3)(I_2 - 3) \quad (11)$$

where I_1 and I_2 are the first and the second invariant of the left Cauchy-Green deformation tensor, and where C_{ij} are empirically determined material constants for a human artery according to [17].

3.1.1. Numerical validation of the backward displacement method

To validate the backward displacement method a zero-pressure geometry is pressurized in a forward analysis by applying a uniformly distributed pressure load of 80 mmHg to the inner surface of the vessel wall. The resulting geometry is taken as the in vivo measured geometry at the diastolic phase and serves as a starting point for the backward problem. This inverse problem is then solved using the backward displacement method in order to restore a zero-pressure geometry which is eventually compared to the original zero-pressure geometry. Upon convergence ($i = n$) the maximum nodal deviation between the original ($\boldsymbol{X}$) and the restored ($\boldsymbol{X}^n = \boldsymbol{X}^*$) zero-pressure geometry is of the same order of magnitude as the maximum residual r^n_{max}.

As defined by (9) and (10) in section 2.2, the maximum residual represents the maximal distance between a node at the originally in vivo measured geometry $\boldsymbol{x}_m$ and the corresponding node resulting from a forward analysis $\boldsymbol{x}^i$ started from the i^{th} approximation of the restored zero-pressure geometry $\boldsymbol{X}^i$. Its evolution throughout the iterative process is shown in Figure 2 in order to evaluate the rate of convergence when solving for the zero-pressure geometry using the backward displacement method. The logarithm of the maximum residual decreases linearly during subsequent iterations until it reaches the machine accuracy.

3.1.2. Evaluation of the effect of in vivo stress incorporation

To evaluate the effect of in vivo stress incorporation, a simulation is performed in which the internal pressure is first set to the end-diastolic pressure (80 mmHg) and subsequently increased to the end-systolic pressure (120 mmHg). This is done for three different setups:

1. The in vivo measured geometry is assumed to be the unloaded geometry. In the forward simulation the in vivo measured geometry is inflated using the physiological pressure values (80 mmHg diastolic pressure; 120 mmHg systolic pressure). The results are visualized in quadrant I.

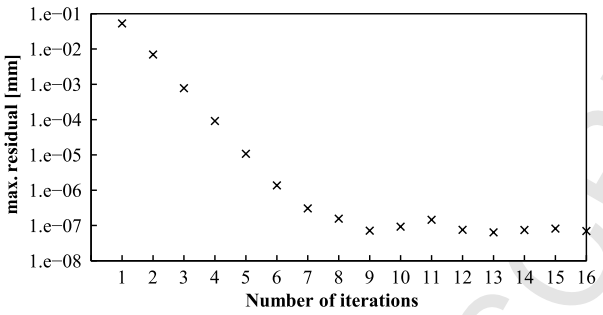

Figure 2: Rate of convergence when solving for the zero-pressure geometry of a thick-walled cylinder (example 1) using the backward displacement method.

2. The in vivo measured geometry is assumed to be the geometry at end-diastole, but neglects the existence of prestress at the diastolic phase. In the forward simulation the in vivo measured geometry is only inflated to 40 mmHg, the end-systolic minus end-diastolic pressure difference. To allow for a fair comparison of the calculated stresses with the other two cases, the stress tensor field was corrected, adding an approximation of the stress field at diastole. The latter resulted from a simulation in which 80 mmHg was applied onto the diastolic geometry. The results are visualized in quadrant IV.
3. The proposed strategy in which the forward simulation towards the physiological pressure values starts from the restored zero-pressure geometry (p_m= 80 mmHg). This results in a prestressed in vivo geometry at diastole. The results are visualized in both quadrant II and III.

Figure 3(a) presents the maximum principal or circumferential stress at end-systole (120 mmHg). The contour plots are shown on the corresponding geometry. Figure 3(b) visualizes the grid of the undeformed reference geometry, together with inner and outer contours of the zero-pressure (black), the end-diastolic (blue dotted line) and the peak-systolic (red dashed line) geometries. Next to the figure the inner radii, the peak-systolic minus end-diastolic radial displacement, and the ratio of the inner radii to the inner radius of the measured geometry (r_m= 0.547 mm) are tabulated for each of the three setups. By definition, note that the measured geometry equals the zero-pressure geometry in setup 1, and the end-diastolic geometry in setup 2 and 3.

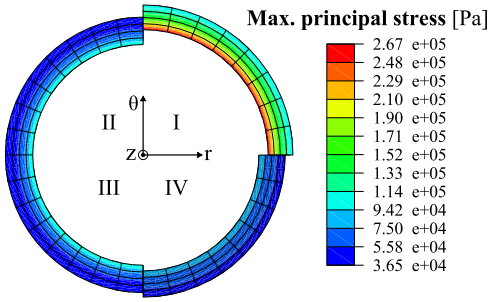

(a)

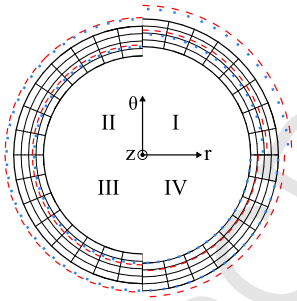

(b)

	setup		
	1 (I)	2 (IV)	3 (II-III)
[mm]			
r_0	0.547	-	0.500
r_d	0.600	0.547	0.547
r_s	0.610	0.585	0.556
r_s-r_d	0.010	0.039	0.009
[%]			
r_0/r_m	100	-	91.46
r_d/r_m	109.67	100	100
r_s/r_m	111.50	107.06	101.64

Figure 3: (a) Contours of the max. principal stress [Pa] at peak-systole. (b) Grid of the undeformed reference geometry, together with inner and outer contours of the zero-pressure (black), the end-diastolic (blue dotted line) and the peak-systolic (red dashed line) geometries. The inner radii of the corresponding contours, the radial end-diastolic to peak-systolic distension and the ratio of the different contours to the measured inner radius (r_m=0.547 mm) are tabulated. For more information about the different quadrants, the reader is referred to the text in section 3.1.2.

Compared to setup 3, the results in Figure 3 clearly show the overestimation of the maximum principal stress when the in vivo measured geometry is assumed to be the unloaded geometry (setup 1). Furthermore, the outer contours of the cross sectional areas at end-diastole and peak-systole are a better approximation when the in vivo geometry is assumed to be the diastolic geometry (setup 2). However, the peak-systolic minus end-diastolic radial displacement in setup 2 is overestimated by a factor of 4.3 due to the nonlinear material law and the absence of prestress/prestrain at the start of the inflation process.

3.2. Example 2: in vivo stress incorporation in a mouse-specific abdominal aorta

In a second example, a more complex cardiovascular structure was created based on contrast-enhanced micro-CT images of the abdominal aorta of an in-house bred male ApoE -/- mouse on a C57BL/6 background (age: 5 months, body weight: 29 g). A mouse-specific 3D geometry of the aortic lumen containing four side branches was obtained in vivo, by segmentation of micro-CT (Triumph, Gamma Medica) images in Mimics (Materialise). In order to obtain sufficient contrast during the imaging process the mouse was intravenously injected with Aurovist (Nanoprobes), a contrast agent which provided satisfying results in earlier studies [18]. Using pyFormex [19] a structured grid was projected onto the outer surface resulting from segmentation yielding a hexahedral mesh for the aortic wall, Figure 4(a), according to the method of De Santis et al. [20]. The mesh

for the aortic wall consists of 80640 elements with 5 elements to represent the wall thickness, 48 elements in the circumferential direction and local refinements in the bifurcation regions, Figure 4(b). The wall thickness was assumed to be 20 percent of the local radius and thus varies throughout the structure.

The element type, the free radial displacement boundary condition at the ending cross sections (3) and the polynomial hyperelastic material model (11) were adopted from the first example (section 3.1). For example purpose only, identical material parameters as in the example of the human vessel were used for the constitutive material law, what can be justified by the fact that the basic constituents of the arterial wall are similar in all mammals.

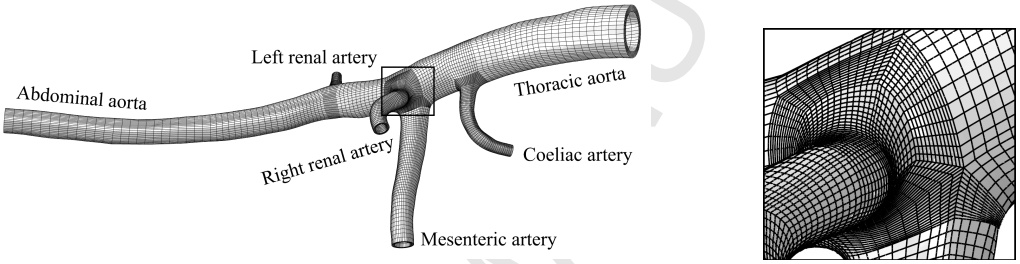

Figure 4: Hexaedral mesh for the arterial wall of the abdominal aorta of a mouse (length sample about 20 mm) and its side branches (a), and a detail of the mesh at the trifurcation region (b).

To further evaluate the backward displacement method this more complex geometry was brought to its zero-pressure state, assuming the internal pressure load at the moment of medical imaging to be 80 mmHg. Afterwards, in vivo stress was computed by reapplying this pressure load in a forward calculation.

The rate of convergence (Figure 5) is plotted for a backward displacement simulation with a convergence criterion set at 0.01% of the mean arterial diameter. Similarly to the convergence rate of the simplified artery in example 1, the logarithm of the maximum residual follows a linear decline after the second iteration. Although the geometry is much more complicated, only a three times less steep slope was found. Remark that the wall clock time of the overall calculation varies linearly with the number of iterations. The proportionality constant is the time required to perform one forward calculation. For this specific case and for a structural solver calculating in parallel on all 12 cores of a Dell PowerEdge R610 server with 2 six-core Intel Xeon X5680 3.33GHz processors and 96GB RAM, the computation time per iteration takes approximately 1270 s.

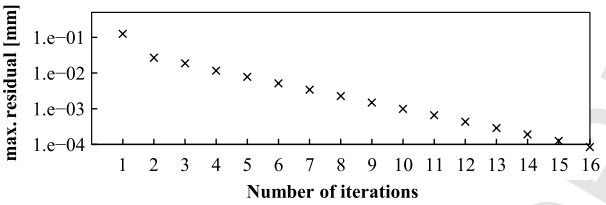

Figure 5: Rate of convergence when solving for the zero-pressure geometry of a mouse-specific abdominal aorta (example 2) using the backward displacement method.

Figure 6 depicts the contour plots of the stress field and the displacement field present in the in vivo measured geometry at the moment of medical imaging. This is the result of applying the end-diastolic pressure on the restored zero-pressure geometry of the more complex cardiovascular structure.

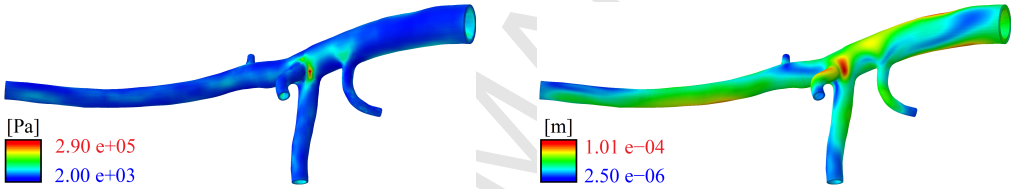

(a) (b)

Figure 6: Contours of (a) the max. principal stress [Pa], and (b) the displacement [m]. Both after applying the internal pressure load, present at the moment of medical imaging, onto the restored zero-pressure geometry.

4. Conclusion

In conclusion, this paper presents a method to restore the original geometry of a structure in absence of its loading state, and to recover the in vivo stress field of the final, loaded structure. Therefore, a given final geometry and a given load are used in a fixed point algorithm in which an iteratively updated displacement field is subtracted from the final reference geometry. The proposed method allows to restore the zero-pressure geometry of in vivo measured cardiovascular structures. To emphasize the importance of prestress in this field of research, the example in section 3.1 shows that the incorporation of in vivo stress in numerical models of arteries is necessary to properly estimate stress and displacement in

the physiological blood pressure range. Furthermore, the convergence rate of the proposed technique is high and decreases only slightly for a much more complex structure using the same constitutive material law. Finally and most importantly, the backward displacement method allows for a straightforward implementation of the algorithm in combination with existing structural solvers as only an update of the mesh coordinates needs to be performed.

Acknowledgements

This research was funded by the Special Research Fund of the Ghent University (BOF10/GOA/005) and by the Research Foundation - Flanders (FWO) project nr. G.0275.08. Joris Degroote gratefully acknowledges funding by a postdoctoral fellowship of the Research Foundation - Flanders (FWO). Bram Trachet is recipient of a research grant of the Flemish government agency for Innovation by Science and Technology (IWT).

References

[1] J. Degroote, I. Couckuyt, J. Vierendeels, P. Segers, T. Dhaene, Inverse modelling of an aneurysms stiffness using surrogate-based optimization and fluid-structure interaction simulations, Structural and Multidisciplinary Optimization (2012) 1–13.

[2] J. Lu, X. Zhou, M. L. Raghavan, Inverse elastostatic stress analysis in pre-deformed biological structures: Demonstration using abdominal aortic aneurysms., Journal of Biomechanics 40 (3) (2007) 693–6.

[3] S. de Putter, B. J. B. M. Wolters, M. C. M. Rutten, M. Breeuwer, F. A. Gerritsen, F. N. van de Vosse, Patient-specific initial wall stress in abdominal aortic aneurysms with a backward incremental method, Journal of Biomechanics 40 (5) (2007) 1081–1090.

[4] M. W. Gee, C. Reeps, H. H. Eckstein, W. A. Wall, Prestressing in finite deformation abdominal aortic aneurysm simulation, Journal of Biomechanics 42 (2009) 1732–1739.

[5] L. Speelman, E. M. H. Bosboom, G. Schurink, J. Buth, M. Breeuwer, M. Jacobs, F. van de Vosse, Initial stress and nonlinear material behavior in patient-specific AAA wall stress analysis, Journal of Biomechanics 42 (11) (2009) 1713 – 1719.

[6] M. Merkx, M. van 't Veer, L. Speelman, M. Breeuwer, J. Buth, F. van de Vosse, Importance of initial stress for abdominal aortic aneurysm wall motion: Dynamic MRI validated finite element analysis, Journal of Biomechanics 42 (14) (2009) 2369 – 2373.

[7] S. Govindjee, P. A. Mihalic, Computational methods for inverse finite elastostatics, Computer Methods in Applied Mechanics and Engineering 136 (1-2) (1996) 47 – 57.

[8] S. Govindjee, P. A. Mihalic, Computational methods for inverse deformations in quasi-incompressible finite elasticity, International Journal for Numerical Methods in Engineering 43 (5) (1998) 821–838.

[9] V. D. Fachinotti, A. Cardona, P. Jetteur, Finite element modelling of inverse design problems in large deformations anisotropic hyperelasticity, International Journal for Numerical Methods in Engineering 74 (6) (2008) 894–910.

[10] M. L. Raghavan, B. Ma, M. Fillinger, Non-invasive determination of zero-pressure geometry of arterial aneurysms, Annals of Biomedical Engineering 34 (2006) 1414–1419.

[11] M. W. Gee, C. Förster, W. A. Wall, A computational strategy for prestressing patient-specific biomechanical problems under finite deformation, International Journal for Numerical Methods in Biomedical Engineering 26 (1) (2010) 52–72.

[12] V. Alastrué, A. Gara, E. Pea, J. F. Rodrguez, M. A. Martnez, M. Doblar, Numerical framework for patient-specific computational modelling of vascular tissue, International Journal for Numerical Methods in Biomedical Engineering 26 (1) (2010) 35–51.

[13] L. Speelman, A. C. Akyildiz, B. den Adel, J. J. Wentzel, A. F. W. van der Steen, R. Virmani, L. van der Weerd, J. W. Jukema, R. E. Poelmann, E. H. van Brummelen, F. J. H. Gijsen, Initial stress in biomechanical models of atherosclerotic plaques, Journal of Biomechanics 44 (13) (2011) 2376 – 2382.

[14] P. M. Pinsky, D. van der Heide, D. Chernyak, Computational modeling of mechanical anisotropy in the cornea and sclera., Journal of cataract and refractive surgery 31 (1) (2005) 136–45.

[15] Y. Bazilevs, M. C. Hsu, Y. Zhang, W. Wang, T. Kvamsdal, S. Hentschel, J. Isaksen, Computational vascular fluid-structure interaction: methodology and application to cerebral aneurysms, Biomechanics and Modeling in Mechanobiology 9 (2010) 481–498.

[16] M. C. Hsu, Y. Bazilevs, Blood vessel tissue prestress modeling for vascular fluid-structure interaction simulation, Finite Elements in Analysis and Design 47 (2011) 593–599.

[17] P. J. Prendergast, C. Lally, S. Daly, A. J. Reid, T. C. Lee, D. Quinn, F. Dolan, Analysis of prolapse in cardiovascular stents: A constitutive equation for vascular tissue and finite-element modelling, Journal of Biomechanical Engineering 125 (5) (2003) 692–699.

[18] B. Trachet, M. Renard, G. De Santis, S. Staelens, J. De Backer, L. Antiga, B. Loeys, P. Segers, An integrated framework to quantitatively link mouse-specific hemodynamics to aneurysm formation in angiotensin II-infused ApoE -/- mice, Annals of Biomedical Engineering 39 (2011) 2430–2444.

[19] http://www.pyformex.org.

[20] G. De Santis, M. De Beule, K. Van Canneyt, P. Segers, P. Verdonck, B. Verhegghe, Full-hexahedral structured meshing for image-based computational vascular modeling, Medical Engineering & Physics 33 (10) (2011) 1318 – 1325.